Journal of Power Sources 196 (2011) 7420–7425

Contents lists available at ScienceDirect

Journal of Power Sources

journal homepage: www.elsevier.com/locate/jpowsour

$SrCo_{1-y}Ti_yO_{3-\delta}$ as potential cathode materials for intermediate-temperature solid oxide fuel cells

Yu Shen, Fang Wang, Xin Ma, Tianmin He*

State Key Laboratory of Superhard Materials, College of Physics, Jilin University, Changchun 130012, China

ARTICLE INFO

Article history:
Received 21 February 2011
Received in revised form 11 April 2011
Accepted 13 April 2011
Available online 20 April 2011

Keywords:
Solid oxide fuel cell
Cathode
Mixed conductor
Strontium cobaltite
Stability
Electrochemical performance

ABSTRACT

The perovskites $SrCo_{1-y}Ti_yO_{3-\delta}$ (SCT*y*, $y = 0.00$–0.20) are synthesized and assessed as potential cathode materials for intermediate-temperature solid oxide fuel cells (IT-SOFCs) based on the $La_{0.9}Sr_{0.1}Ga_{0.8}Mg_{0.2}O_{3-\delta}$ (LSGM) electrolyte. SCT*y* composites with $y \geq 0.05$ adopt a cubic perovskite structure with thermal stability between 30 °C and 1000 °C in air. Substitution of Ti significantly enhances the electrical conductivity of the SCT*y* composites relative to the undoped $SrCoO_{3-\delta}$. The highest electrical conductivity of the sample with $y = 0.05$ varied from 430 S cm^{-1} to 160 S cm^{-1} between 300 °C to 800 °C in air. The area-specific resistances of the SCT*y* cathodes on the LSGM electrolyte gradually increase from 0.084 Ω cm^2 at $y = 0.05$ to 0.091 Ω cm^2 at $y = 0.20$ with increasing Ti content at 750 °C. Single-cells that used SCT*y* cathodes with $y = 0.05$, 0.10, 0.15, and 0.20 on a 300 μm-thick LSGM electrolyte achieve peak power densities of 793, 608, 525, and 425 mW cm^{-2} at 800 °C, respectively. These novel SCT*y* cubic perovskites demonstrate considerable potential for application in IT-SOFC cathodes.

1. Introduction

Mixed ionic and electronic conductors have attracted considerable attention due to their potential technological applications in oxygen separation membranes, syngas production, gas sensors, and solid oxide fuel cell (SOFC) cathodes [1,2]. $SrCoO_{3-\delta}$ oxide is an important parent compound of functional materials that have multiple phase structures. It exhibits three polymorphs, namely, the orthorhombic brownmillerite phase between room temperature and 653 °C, the hexagonal phase between 653 °C and 920 °C, and the cubic perovskite phase above 920 °C, which reverts to the hexagonal phase when cooled down to 774 °C [3]. Among the various phase structures, the cubic perovskite phase shows the highest electronic and ionic conductivity [4]. The electronic conductivity of $SrCoO_{3-\delta}$ cubic perovskite exceeds the conductivity of the low-temperature phase by one order of magnitude [5]. However, the reversible transition to the hexagonal phase occurs at temperatures below 920 °C. This transition also leads to the modification of electronic behavior of $SrCoO_{3-\delta}$ cubic perovskite, which affects the transport properties of this material [6]. Further studies have demonstrated that the hexagonal phase at room temperature is almost impermeable to oxygen [7]; this limits its application in the aforementioned electrochemical devices. Therefore, the stabilization of the cubic phase at room temperature is necessary to use effectively $SrCoO_{3-\delta}$ oxide for various technological applications. Extensive research has been performed to improve the stability of this phase [8–18]. Solid solutions of $SrCoO_{3-\delta}$ oxide with cubic perovskite structure have been successfully applied in intermediate-temperature solid oxide fuel cells (IT-SOFCs) as a cathode [19–26].

Nagai et al. reported that various cations that substituted Co in $SrCoO_{3-\delta}$ oxide produced perovskites with decreasing stability in the following order: Nb > Ti > Fe > La > V [11]. Our recent studies have suggested that the $SrCo_{1-y}Nb_yO_{3-\delta}$ materials not only possess high stability, but also display good cathodic performance in the IT-SOFCs when $y \geq 0.10$ [20]. To extend our work, we studied the properties of $SrCo_{1-y}Ti_yO_{3-\delta}$ oxides as potential cathode materials for IT-SOFCs. The effects of Ti substitution in the Co site on the phase structure, electrical conductivity, thermal expansion behavior, and cathode performance was investigated. The performance of cells using $SrCo_{1-y}Ti_yO_{3-\delta}$ ($y = 0.05$–0.20) cathodes in an $LaGaO_3$-based electrolyte is also presented.

2. Materials and methods

2.1. Preparation of materials

The $SrCo_{1-y}Ti_yO_{3-\delta}$ (SCT*y*, $y = 0.00$–0.20) oxides were synthesized via a solid-state reaction using $SrCO_3$ (99%), Co_3O_4 (99%), and TiO_2 (98%) as raw materials. Stoichiometric amounts of raw materials were mixed thoroughly, and the mixtures were pressed

* Corresponding author: Tel.: +86 431 85166112; fax: +86 431 85166112.
E-mail addresses: hetm@jlu.edu.cn, hly@mail.jlu.edu.cn (T. He).

0378-7753/$ – see front matter © 2011 Elsevier B.V. All rights reserved.
doi:10.1016/j.jpowsour.2011.04.025

into pellets and calcined repeatedly at 1000 and 1100 °C for 10 h in air, with intermediate grinding. The calcined samples were reground, pressed into pellets (13 mm diameter, 1 mm thickness) and cylinders (6 mm diameter, 5–7 mm thickness) at 220 MPa for the electrical conductivity and thermal expansion measurements, and were finally sintered at 1200 °C for 10 h in air. The $La_{0.9}Sr_{0.1}Ga_{0.8}Mg_{0.2}O_{3-\delta}$ (LSGM), $Ce_{0.8}Sm_{0.2}O_{1.9}$ (SDC) and NiO powders were synthesized through the glycine–nitrate process [27]. The dense LSGM electrolyte pellets were prepared by sintering the samples at 1450 °C for 10 h. The NiO/SDC composite anode was obtained by mixing NiO powder with SDC powder at a weight ratio of 65:35 (NiO:SDC).

2.2. Characterization of materials and cell test

The crystalline structures of the synthesized samples were characterized by XRD using Cu Kα radiation (Rigaku-D-Max γA, λ = 0.15418 nm). The XRD patterns were obtained at room temperature by step scanning in the range of $20° \le 2\theta \le 80°$ at an increment of 0.02°. The thermal expansion coefficient (TEC) was measured in sintered cylinders with a push-rod dilatometer (Netzsch DIL 402C) in the temperature range of 30–1000 °C at a heating rate of 5 °C min^{-1}, using Al_2O_3 as the reference. Air was used as purge gas, and the flow rate was controlled at 60 mL min^{-1}. The electrical conductivity of the sample was measured between 50 °C and 850 °C in air, using the van der Pauw method.

For the electrochemical performance studies, symmetrical cells of SCT*y*/LSGM/SCT*y* were prepared by screen printing SCT*y* slurry onto both sides of the LSGM electrolyte pellets, followed by calcining at 950 °C for 2 h in air. The a.c. impedance spectroscopy was performed using an electrochemical analyzer (CHI604D, Chenhua) over the temperature range 650–800 °C, in air. The frequency range for the a.c. impedance measurement was from 0.1 Hz to 100 kHz, and the signal amplitude was 10 mV. The electrolyte-supported single-cell was fabricated using 300 μm-thick LSGM electrolyte pellets, SCT*y* as cathode, and NiO/SDC as anode. To prevent a chemical reaction between Ni in the anode and the LSGM electrolyte during sintering, an SDC interlayer was first introduced between the electrolyte and the anode, and was sintered at 1300 °C for 1 h. The anode was screen-painted onto the SDC interlayer and subsequently sintered at 1250 °C for 4 h in air. Similarly, the SCT*y* cathode was screen-painted onto the opposite side of the LSGM pellets and calcined at 950 °C for 2 h. The single-cell performance was tested at various temperatures using dry hydrogen as fuel and ambient air as oxidant.

3. Results and discussion

3.1. Phase structure

Fig. 1 shows the room-temperature XRD patterns of the SCT*y* samples (*y* = 0.00–0.20) sintered in air at 1200 °C for 10 h. A significant difference was observed between the XRD patterns of the undoped $SrCoO_{3-\delta}$ and SCT*y* (*y* = 0.05–0.20) samples. The undoped $SrCoO_{3-\delta}$ adopted a hexagonal phase with the distorted 2H–$BaNiO_3$-type structure [3,4,11], whereas the Ti-substituted $SrCoO_{3-\delta}$ at *y* = 0.05–0.20 crystallized in a cubic perovskite structure. This variation suggests that the substitution of Ti for Co in the SCT*y* oxides ($0.05 \le y \le 0.20$) efficiently stabilized the cubic perovskite phase at room temperature, which was in good agreement with the previous report of Kharton et al. [8]. The unit-cell parameters of SCT*y* oxides with various Ti substitution contents were calculated based on the cubic perovskite structure at room temperature (Table 1). The unit-cell parameters of the SCT*y* oxides increased with increasing Ti content. The ionic radii of

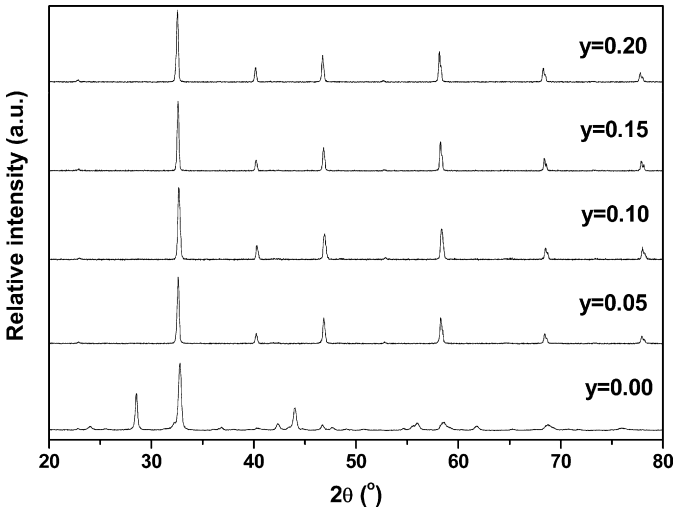

Fig. 1. Room-temperature XRD patterns of the SCT*y* samples (*y* = 0.00–0.20) sintered at 1200 °C for 10 h in air.

Table 1
Unit-cell parameters and TECs of the SCT*y* materials.

Sample *y*	Unit-cell parameters		TEC × 10^{-6} (K^{-1})		
	a (nm)	*V* (nm^3)	30–400 °C	400–1000 °C	30–1000 °C
0.05	0.38754	0.05820	18.3	23.0	21.2
0.10	0.38725	0.05807	18.9	25.4	22.9
0.15	0.38780	0.05832	18.1	24.7	22.2
0.20	0.38799	0.05841	19.1	25.3	23.0

the Co^{3+}/Co^{4+} and Ti^{3+}/Ti^{4+} in six-coordination are 0.061/0.053 and 0.0670/0.0605 nm, respectively [28]. Therefore, the unit-cell parameters of SCT*y* are expected to increase with increasing Ti content due to the substitution of the smaller Co ions by the larger Ti ions. Similar trends in the unit-cell parameters were also observed in the SCT*y* oxides reported by Kharton et al. [8].

3.2. Thermal expansion and phase stability

Fig. 2 shows the thermal expansion curves of the SCT*y* samples between 30 °C and 1000 °C in air. The thermal expansion curve of the undoped $SrCoO_{3-\delta}$ sample is distinctly different from those

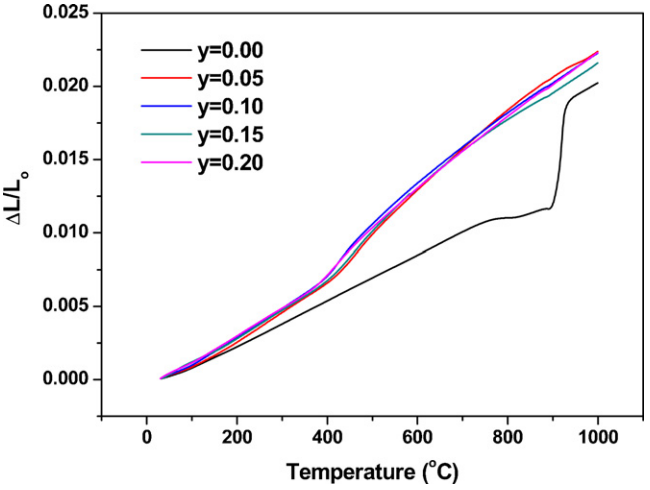

Fig. 2. Thermal expansion curves of the SCT*y* samples (*y* = 0.00–0.20) between 30 °C and 1000 °C in air.

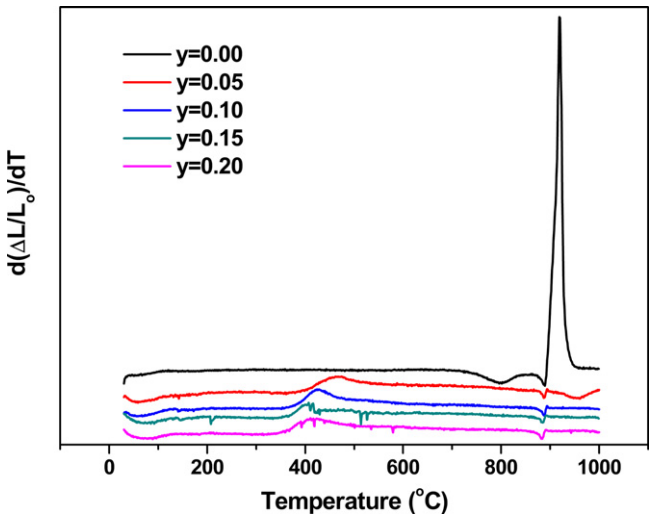

Fig. 3. Differential curves of $\Delta L/L_0$ against temperature for the SCTy samples (y = 0.00–0.20) in air.

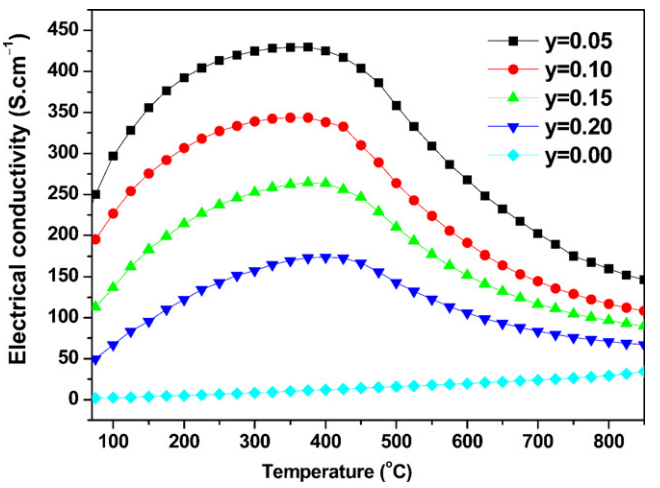

Fig. 4. Temperature dependence of the electrical conductivity of the SCTy samples (y = 0.00–0.20).

of the SCTy (y = 0.05–0.20) samples. This is mainly attributable to the three polymorphs of undoped $SrCoO_{3-\delta}$ oxide at the range of room temperature to 1200 °C [3]. The SCTy (y = 0.05–0.20) samples showed linear expansion in the low-temperature range (30–400 °C) and high-temperature range (400–1000 °C), and the slope of the linear expansion curves increased at high temperatures. The increased slope is due to the loss of oxygen from the lattice at high temperatures and the consequent change from the smaller ionic radius of Co^{4+} to the larger the ionic radii of Co^{3+} or Co^{2+}, which has been demonstrated by TGA [20,24,29,30]. The average TEC values were calculated from the two temperature ranges (Table 1). The average TEC values of the SCTy system are still higher within 30–1000 °C (Table 1) than the typical ranges for SOFCs, but they fall within the range of those of other cobalt-based perovskite cathodes [2,31,32]. Similar thermal expansion behavior has been observed in the $SrCo_{1-y}Nb_yO_{3-\delta}$ [20] and $SrCo_{1-x}Sb_xO_{3-\delta}$ [24] materials.

Fig. 3 presents the differential curves of $\Delta L/L_0$ against temperature for the SCTy samples between 30 °C and 1000 °C. The plots demonstrate clearly the thermal stability and the variation in phase-transition temperature of the SCTy system. At 920 °C, a sudden change corresponding to the hexagonal-to-cubic structural phase-transition occurs in the differential curves of the undoped $SrCoO_{3-\delta}$ sample [3]. However, no markedly abrupt changes attributable to structural phase-transitions were observed at around 920 °C for the SCTy samples with y = 0.05–0.20. These trends suggest that the structural phase-transition in SCTy oxides could be efficiently inhibited by the substitution of Ti for Co, which is in good agreement with the aforementioned XRD study. In addition, a weak abrupt change was observed at around 400 °C in the differential curves of $\Delta L/L_0$ versus temperature for the SCTy (y = 0.05–0.20) samples. This corresponds to the reduction of Co^{4+} to Co^{3+} and the loss of oxygen from the lattice [20,24,29,30]. Interestingly, the phase-transition temperature shifted from ~460 °C for y = 0.05 to ~400 °C for y = 0.20 with increasing Ti content. This is mainly because the substitution of Co by Ti in SCTy weakens the Co–O bond and allows easier release of oxygen when the SCTy samples are heated [33]. Therefore, the phase-transition temperatures observed in samples decreased with increasing Ti content. A similar decrease in the phase-transition temperature of $SrCo_{1-y}Nb_yO_{3-\delta}$ has been observed in our latest study [20].

3.3. Electrical conductivity

Fig. 4 shows the temperature dependence of electrical conductivity of the SCTy samples (y = 0.00–0.20) in air. The electrical behavior of the undoped hexagonal $SrCoO_{3-\delta}$ is different from those of SCTy (y = 0.05–0.20). The undoped sample behaved similarly to a semiconductor, since its conductivity increased from 1.5 S cm^{-1} to 34 S cm^{-1} between 50 °C and 850 °C. The substitution of Ti for Co significantly improved the electrical conductivity of the SCTy (y = 0.05–0.20) samples because the high-temperature cubic phase was stabilized at room temperature, as confirmed from the XRD and thermal expansion studies. The conductivity of the SCTy samples was lower compared with those of the $SrCo_{1-y}Nb_yO_{3-\delta}$ materials (182, 145, 112, and 82 S cm^{-1} at 800 °C for y = 0.05, 0.10, 0.15. and 0.20, respectively [20]). However, all SCTy samples (y = 0.05–0.20) showed conductivity > 71 S cm^{-1} between 600 °C and 800 °C, which is acceptable for materials used as cathodes in IT-SOFCs.

A semiconductor-like to metallic-like transition, observed at about 400 °C for the SCTy (y = 0.05–0.20) samples (Fig. 4), is associated with the reduction from Co^{4+} to Co^{3+} and the oxygen loss from the lattice, as demonstrated by the thermal expansion study. The conductivity values of the samples reached the maximum 174–430 S cm^{-1} at about 400 °C, and then decreased at higher temperatures. Similar results have been reported in the $SrCo_{1-y}Nb_yO_{3-\delta}$ and $SrCo_{1-y}Sb_yO_{3-\delta}$ systems [20,24]. The formation of the cubic perovskite phase significantly improved the electrical conductivity of the SCTy (y = 0.05–0.20) samples. The sample with y = 0.05 had the highest electrical conductivity (430 S cm^{-1} at 375 °C). However, the electrical conductivity decreased with further increase in the Ti content. The electronic conduction process in the $SrCoO_{3-\delta}$-based cubic perovskites proceeds through hopping between the oxygen ion and the adjacent Co-site cations along the Co^{4+}–O^{2-}–Co^{3+} network due to the overlapping between the Co:3d and O:2p orbitals [4]. With an increase in the Ti content in SCTy oxides, the amount of non-conducting Ti–O bonds progressively increase, whereas the conducting Co–O bonds decrease. This hampers the electronic transport [20,24] and results in a decrease in electrical conductivity.

3.4. Area-specific resistance

The electrochemical performance of the SCTy cathodes was assessed by a.c. impedance spectroscopy on a symmetrical cell of SCTy/LSGM/SCTy at various temperatures. Fig. 5 shows the typical impedance spectra of the SCTy cathode (y = 0.05) on the

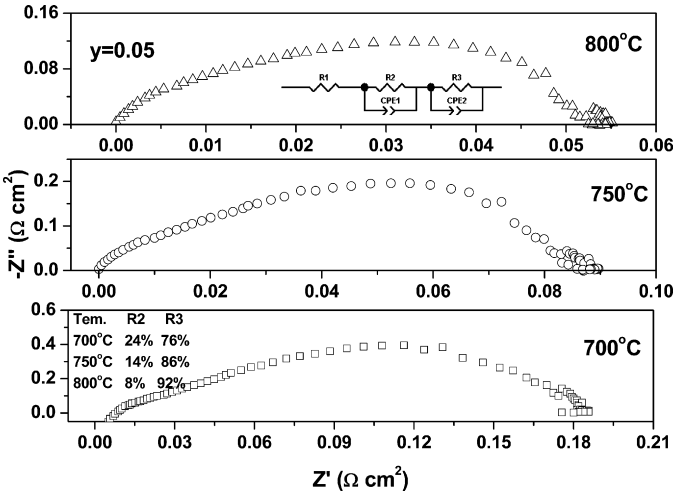

Fig. 5. Typical impedance spectra of the SCT*y* cathode ($y = 0.05$) on the LSGM electrolyte, measured at 700–800 °C in air. The ohmic resistance was subtracted from the experimental data.

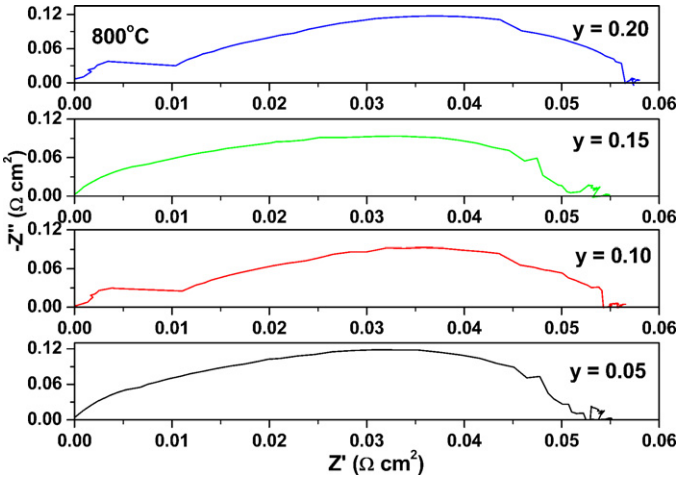

Fig. 7. Typical impedance spectra of the SCT*y* cathodes ($y = 0.05$–0.20) measured at 800 °C in air. The ohmic resistance was subtracted from the experimental data.

LSGM electrolyte at 700–800 °C in air. Similar impedance spectra were also observed for other samples with $y = 0.10$–0.20. The impedance data were fitted by the Z-view software using the equivalent circuit shown in the inset of Fig. 5. The impedance response comprises two distinct depressed arcs in the high and low frequencies, which correspond to at least two electrode processes (Fig. 5). The high-frequency intercept represents the ohmic resistance of the cell, whereas the low-frequency intercept represents the total resistance of the cell. The area-specific resistance (ASR) was estimated from the difference between the high- and low-frequency intercepts in the impedance spectra. The overall ASR includes two cathode–electrolyte interface resistances for the symmetrical cell. The overall ASR was divided by two to obtain the single cathode–electrolyte interface resistance. The ASR values of SCT*y* ($y = 0.05$–0.20) cathodes on the LSGM electrolyte between 700 °C and 800 °C are shown in Fig. 6. The ASR values were significantly reduced with increasing temperature. For example, the ASRs decreased from 0.17 Ω cm^2 at 700 °C to 0.084 Ω cm^2 at 750 °C, to 0.054 Ω cm^2 at 800 °C for the cathode with $y = 0.05$. Moreover, at a given temperature, the ASRs of the SCT*y* cathodes increased with the Ti content from $y = 0.05$ to 0.20 (Fig. 7). These trends are due to the decrease in the oxygen vacancy content and electrical conductivity in the SCT*y* samples with increasing Ti content. Kharton et al. demonstrated by examining the ceramic densities that the oxygen vacancy of the SCT*y* samples decreased with increasing Ti content [8], and resulted in the decrease of oxygen reduction reaction in the cathodes.

To further identify the contribution of the aforementioned two processes, the ASR values of each process were obtained by fitting the impedance data with the equivalent circuit (Fig. 5). The high-frequency resistance R2 is related with the charge-transfer process. The low-frequency resistance R3 is attributed to the diffusion processes [24]. The high-frequency resistance R2 is consistently lower than the low-frequency resistance R3. This suggests that the charge-transfer process is the rate limiting step in the overall polarization process. A similar trend in each polarization contribution has also been reported for the $SrCo_{1-x}Sb_xO_{3-\delta}$ cathodes [24]. In addition, the R2 value decreases and the R3 value increases with increasing temperature, respectively. This is mainly due to the reduction of the electrical conductivities and the increase of the oxygen vacancies in the SCT*y* samples as the temperature is increased.

Fig. 8 shows the Arrhenius plots of the ASR values for SCT*y* cathodes ($y = 0.05$–0.20) on the LSGM electrolyte. The activation energies, calculated from the slope of the fitted line, are 132.0, 117.5, 122.0, and 126.4 kJ mol^{-1} for cathodes with $y = 0.05$, 0.10, 0.15, and 0.20, respectively. The activation energies of ASR for the

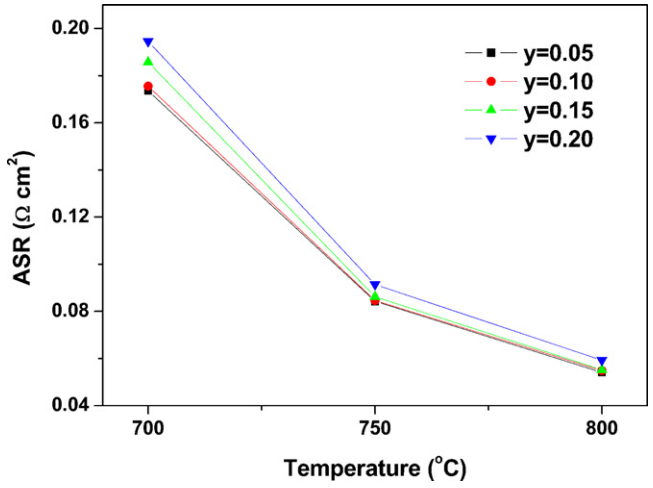

Fig. 6. Variations in the ASR values with temperature for the SCT*y* cathodes ($y = 0.05$–0.20).

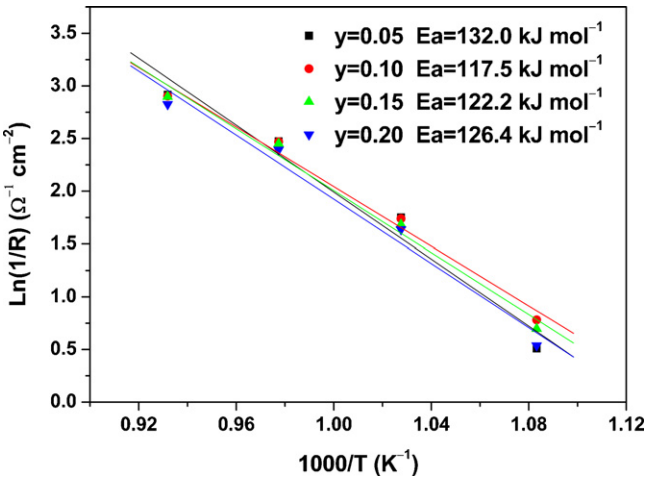

Fig. 8. Arrhenius plots of the ASR values for SCT*y* cathodes ($y = 0.05$–0.20).

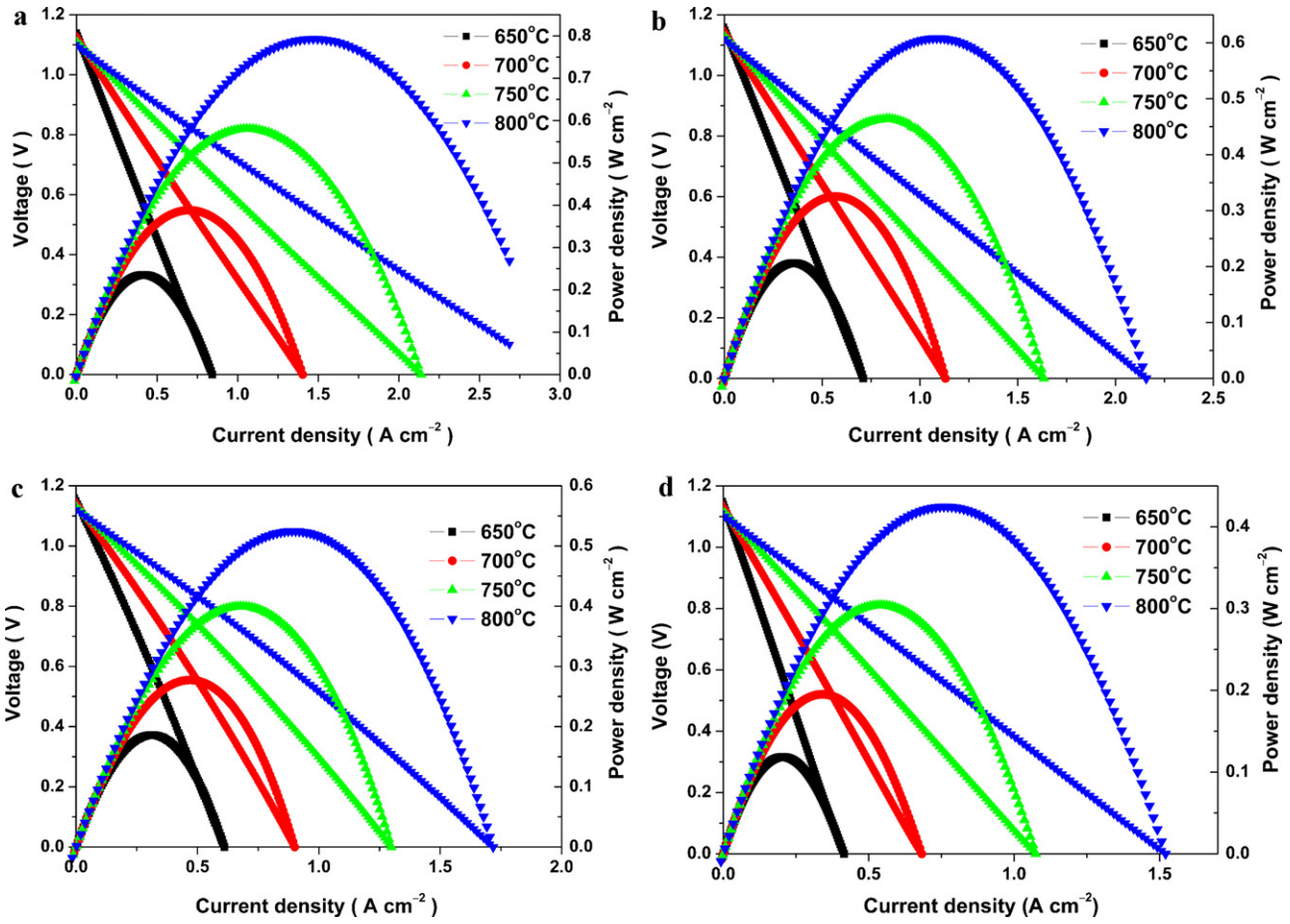

Fig. 9. Electrochemical performance data of the NiO-SDC/SDC/LSGM/SCT*y* single cells using dry H_2 as fuel and ambient air as oxidant in the temperature range of 650–800 °C: (a) $y = 0.05$, (b) $y = 0.10$, (c) $y = 0.15$ and $y = 0.20$.

SCT*y* cathodes are higher than the activation energies of 104.4, 98.9, and 93.9 kJ mol^{-1} for the $SrCo_{1-y}Nb_yO_{3-\delta}$ cathodes at $y = 0.10$, 0.15, and 0.20, respectively [20]. The higher activation energy can be attributed primarily to the lower conductivity of the SCT*y* cathodes compared with those of the $SrCo_{1-y}Nb_yO_{3-\delta}$ cathodes, as discussed in Section 3.3.

3.5. Cell performance

Fig. 9 demonstrates the variation in cell voltage and power density as a function of current density for NiO-SDC/SDC/LSGM/SCT*y* cells between 650 °C and 800 °C. The power densities of the cells with $y = 0.05$, 0.10, 0.15, and 0.20 reached maxima of 793, 608, 525, and 425 mW cm^{-2} at 800 °C, respectively. Data for maximum power density of the cells at various temperatures are shown in Fig. 10. The maximum power density decreased with increasing Ti content for a given temperature; this is in good agreement with the electrical conductivities and impedance spectra previously discussed. The cell performance of the SCT*y* cathodes was lower than that of the $SrCo_{1-y}Nb_yO_{3-\delta}$ cathodes in a recent report [20]. This characteristic can be attributed mainly to the reduction of the electrical conductivity and the increase of ASR in the SCT*y* cathodes relative to those of the $SrCo_{1-y}Nb_yO_{3-\delta}$ cathodes. However, the cell performance observed in the present study is comparable to those of cells that use $SrCo_{1-y}Nb_yO_{3-\delta}$ cathodes; these may be particularly significant for applications in IT-SOFCs. In particular, the SCT*y* at $y = 0.05$ cathode displayed excellent performance. This suggests that SCT*y* is a candidate for use in cathode materials in IT-SOFCs.

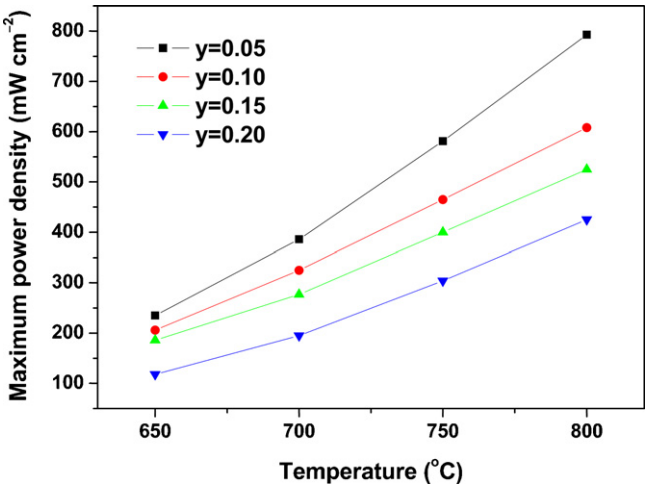

Fig. 10. Variations in the maximum power density with Ti content at different temperatures.

4. Conclusions

The SCT*y* ($y = 0.00$–0.20) perovskites were assessed as potential cathode materials for IT-SOFCs on LSGM electrolyte. The substitution of Co by Ti in the SCT*y* oxides ($y = 0.05$–0.20) not only efficiently stabilized the high-temperature cubic perovskite phase of these compounds at room temperature, but also greatly improved their electrical conductivity. The electrical conductivities of the sam-

ples with $y = 0.05$–0.20 were 160–268, 117–191, 96–152, and 71–106 S cm^{-1} between 600 °C and 800 °C. The electrochemical performance of the SCTy cathodes decreased with increasing Ti content. At 800 °C, the maximum power densities of the cells that used cathodes with $y = 0.05$, 0.10, 0.15, and 0.20 reached 793, 608, 525, and 425 mW cm^{-2}, respectively. These characteristics suggest that SCTy oxides are promising candidate materials for cathodes in IT-SOFCs. Given that SCTy oxides were observed to have higher TECs, lowering the TECs of these materials are the ultimate concerns for practical application in IT-SOFC cathodes.

Acknowledgment

This work was supported by the Natural Science Foundation of China under Contract No. 10974065.

References

[1] P.N. Dyer, R.E. Richards, S.L. Russek, D.M. Taylor, Solid State Ionics 134 (2000) 21–33.
[2] E.V. Tsipis, V.V. Kharton, J. Solid State Electrochem. 12 (2008) 1367–1391.
[3] C. de la Calle, A. Aguadero, J.A. Alonso, M.T. Fernández-Díaz, Solid State Sci. 10 (2008) 1924–1935.
[4] Z.Q. Deng, W.S. Yang, W. Liu, C.S. Chen, J. Solid State Chem. 179 (2006) 362–369.
[5] V.V. Vashook, M.V. Zinkevich, H. Ullmann, J. Paulsen, N. Trofimenko, K. Teske, Solid State Ionics 99 (1997) 23–32.
[6] Y. Takeda, R. Kanno, T. Takada, O. Yamamoto, M. Takano, Y. Bando, Z. Anorg, Allg. Chem. 540/541 (1986) 259–270.
[7] H. Kruidhof, H.J.M. Bouwmeester, R.H.E.V. Doorn, A.J. Burggraaf, Solid State Ionics 816 (1993) 63–65.
[8] V.V. Kharton, A.A.P. Viskup, E.N. Naumovich, A.A. Tonoyan, Mater. Chem. Phys. 53 (1998) 6–12.
[9] V.V. Kharton, A.E.N. Naumovich, Solid State Ionics 96 (1997) 141–151.
[10] W. Ito, T. Nagai, T. Sakon, Solid State Ionics 178 (2007) 809–816.
[11] T. Nagai, W. Ito, T. Sakon, Solid State Ionics 177 (2007) 3433–3444.
[12] P.Y. Zeng, R. Ran, Z.H. Chen, W. Zhou, H.X. Gu, Z.P. Shao, S.M. Liu, J. Alloys Compd. 455 (2008) 465–470.
[13] P.Y. Zeng, Z.P. Shao, S.M. Liu, Z.P. Xu, Sep. Purif. Technol. 67 (2009) 304–311.
[14] M. James, D. Cassidy, K.F. Wilson, J. Horvat, R.L. Withers, Solid State Sci. 6 (2004) 655–662.
[15] K. Zhang, R. Ran, L. Ge, Z.P. Shao, W.Q. Jin, N.P. Xu, J. Membr. Sci. 323 (2008) 436–443.
[16] X.L. Dong, Z. Xu, X.F. Chang, C. Zhang, W.Q. Jin, J. Am. Ceram. Soc. 90 (2007) 3923–3929.
[17] Q.T. Wei, R.S. Guo, F.H. Wang, H.L. Li, J. Mater. Sci. 40 (2005) 1317–1319.
[18] P.Y. Zeng, R. Ran, Z.H. Chen, H.X. Gu, Z.P. Shao, AIChE J. 53 (2007) 3116–3124.
[19] W. Zhou, Z.P. Shao, R. Ran, R. Cai, Electrochem. Commun. 10 (2008) 1647–1651.
[20] F. Wang, Q.J. Zhou, T.M. He, G.D. Li, H. Ding, J. Power Sources 195 (2010) 3772–3778.
[21] Y.B. Zhou, B.M. An, Y.M. Guo, R. Ran, Z.P. Shao, Electrochem. Commun. 11 (2009) 2216–2219.
[22] B. Lin, S.L. Wang, H.L. Liu, K. Xie, H.P. Ding, M.F. Liu, G.Y. Meng, J. Alloys Compd. 472 (2009) 556–558.
[23] A. Aguadero, C. de la Calle, J.A. Alonso, M.J. Escudero, M.T. Fernández-Díaz, L. Daza, Chem. Mater. 19 (2007) 6437–6444.
[24] A. Aguadero, D. Pérez-Coll, C. de la Calle, J.A. Alonso, M.J. Escudero, L. Daza, J. Power Sources 192 (2009) 132–137.
[25] A. Aguadero, J.A. Alonso, D. Pérez-Coll, C. de la Calle, M.T. Fernández-Díaz, J.B. Goodenough, Chem. Mater. 22 (2010) 789–798.
[26] W. Zhou, W.Q. Jin, Z.H. Zhu, Z.P. Shao, Int. J. Hydrogen Energy 35 (2010) 1356–1366.
[27] L.G. Cong, T.M. He, Y. Ji, P.F. Guan, Y.L. Huang, W.H. Su, J. Alloys Compd. 348 (2003) 325–331.
[28] R.D. Shannon, Acta Crystallogr. A 32 (1976) 751–767.
[29] L.W. Tai, M.M. Nasrallah, H.U. Anderson, D.M. Sparlin, S.R. Sehlin, Solid State Ionics 76 (1995) 259–271.
[30] G.Ch. Kostogloudis, N. Vasilakos, Ch. Ftikos, Solid State Ionics 106 (1998) 207–218.
[31] H. Ullmann, N. Trofimenko, F. Tietz, D. Stöver, A. Ahmad-Khanlou, Solid State Ionics 138 (2000) 79–90.
[32] Q.J. Zhou, F. Wang, Y. Shen, T.M. He, J. Power Sources 195 (2010) 2174–2181.
[33] I.D. Brown, R.D. Shannon, Acta Crystallogr. A 29 (1973) 266–282.